https://doi.org/10.5194/wes-2025-226
Preprint. Discussion started: 12 November 2025
© Author(s) 2025. CC BY 4.0 License.

WIND ENERGY SCIENCE DISCUSSIONS

Digital Twin – Driven Machine Learning Optimization Framework for Multizone Curing Control in Wind Turbine Blade Manufacturing

Sahil Kamath[1], Niloufar Adab[1], Rajat Srivastava[1], Zhiqi Mao[1], Ehsan Mehrdad[1], Yingjian Liu[1], Stephen Nolet[2], Joseph Wilson[2], Xu Chen[3], Hongbing Lu[1], Dong Qian[1],

[1]Department of Mechanical Engineering, The University of Texas at Dallas, Richardson, TX
[2]TPI Composites, Inc., Warren, Rhode Island, USA
[3]GE Renewable Energy, Greenville, USA
Correspondence to: Dong Qian (dong.qian@utdallas.edu)

Abstract. The Vacuum-Assisted Resin Infusion Molding (VARIM) process is widely used in wind turbine blade manufacturing due to its cost-effectiveness and reliability. However, challenges such as prolonged curing cycles and defects caused by non-uniform cure remain persistent. To address these issues, multizone heating systems have been developed to enable independent temperature control across blade sections. Yet, optimizing the temperature profile in each zone is computationally intensive, requiring detailed modelling of curing kinetics and heat transfer mechanisms. To overcome these challenges, in this work, a machine learning (ML) based digital twin of the VARIM process was developed using a time-distributed long short-term memory (LSTM) network trained on data generated by a high-fidelity multiphysics solver. The model achieved a predictive accuracy of 96.7% in replicating the resin curing behavior. Its time-distributed architecture effectively captures the spatial - temporal dependencies across multiple zones, allowing precise prediction of the degree-of-cure evolution. Paired with a gradient-free optimization algorithm, the digital twin reduced curing time by 12.5% while improving cure uniformity. This AI-driven framework eliminates costly trial-and-error experimentation, and provides a scalable, adaptive solution for improving both quality and productivity in wind turbine blade manufacturing, with strong potential for extension to other composite manufacturing processes.

https://doi.org/10.5194/wes-2025-226
Preprint. Discussion started: 12 November 2025
© Author(s) 2025. CC BY 4.0 License.

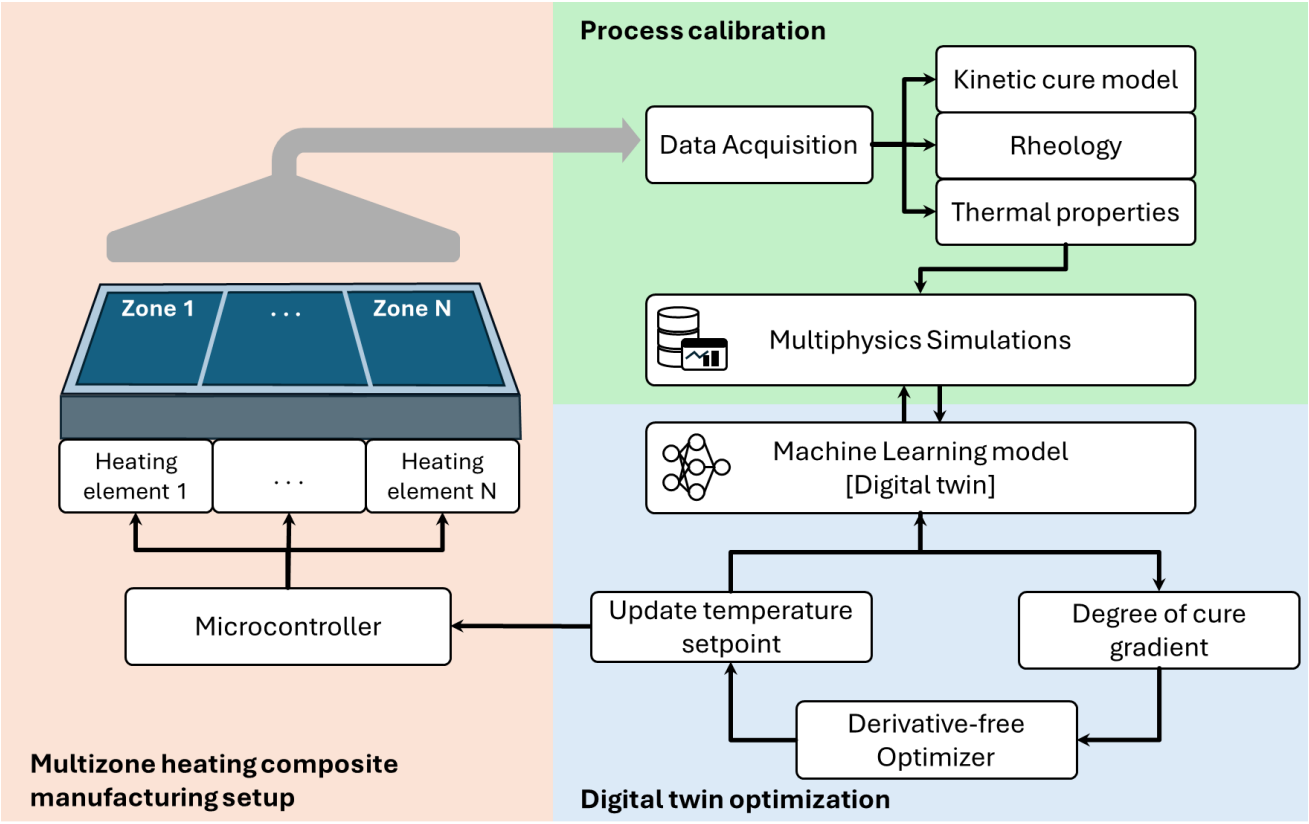

1 Introduction

Wind turbines are a cornerstone of sustainable energy generation, yet their operational reliability remains critical to maintaining consistent power output and minimizing maintenance costs. Failures in major components, such as blades, gearboxes, and generators, can lead to extended downtime and reduced energy efficiency. Improving design strategies, material performance, and process monitoring is therefore essential for extending turbine lifespan, improving operational efficiency, and supporting the long-term viability of wind energy infrastructure.

Among existing manufacturing techniques, the Vacuum-Assisted Resin Infusion Molding (VARIM) process is widely adopted for fabricating large composite wind turbine blades. In this process, dry fiber reinforcements, such as glass or carbon fabrics, and core materials, are first placed in a mold, which is then sealed with a vacuum bag. After evacuation creates negative pressure, low-viscosity resin is drawn through the fiber lay-up to achieve complete impregnation. The infused laminate is subsequently cured under controlled heating, typically using a heated bed or autoclave, to form a stiff composite structure. VARIM enables cost-effective production of large blades with high structural integrity; however, it also presents challenges, including prevention of dry spots, achieving resin flow uniformity, and ensuring uniform curing across regions of the blade with varying thicknesses.

https://doi.org/10.5194/wes-2025-226
Preprint. Discussion started: 12 November 2025
© Author(s) 2025. CC BY 4.0 License.

During the manufacturing, several factors, including mold temperature (Kedari et al., 2011), thermal stresses and chemical shrinkage during curing (Wisnom et al., 2006), thermal oxidation (Upadhyaya et al., 2013), and differences in thermal expansion between fiber and resin (Fu and Yao, 2022) affects the material properties of the final composite product. Because wind turbine blades are composed of layers with varying thermal properties and thicknesses, the resulting non-uniform heating often lead to uneven curing. Such thermal and cure non-uniformities in the VARIM process generate cure-induced temperature gradients, local exotherms, and differential shrinkage, which subsequently produce residual stresses, voids, and interlaminar delamination in the composite structures.

These defects originate during both manufacturing and post-curing stages and significantly accelerate crack initiation under cyclic loading (Struzziero et al., 2020). Manufacturing-induced voids and cure-related porosity act as stress concentrators that evolve into critical damage sites under service conditions. Coupled heat transfer and fracture analyses reveal that such voids amplify local heating and embrittlement, thereby increasing the likelihood of catastrophic failure (Zhou et al., 2020). Field investigations and comprehensive reviews have identified manufacturing and repair-induced defects as dominant root causes of blade failure, strongly correlating with high rates of in-service damage, unexpected repairs, and premature retirements (Mishnaevsky, 2022).

In particular, non-uniform degree of cure in thick or geometrically complex regions poses a high risk of failure. Asymmetric repair-patch exotherms and peak temperature differentials can cause local overheating and cure non-uniformity, which are directly linked to cracking (Shah et al., 2023). Similarly, non-uniform thermal cycles during curing generate residual stresses that initiate cracking and delamination in large composite components (Maduro, 2021), while thermochemical simulations confirm that higher heating rates lead to increased temperature non-uniformities and cure-related defects (Wang et al., 2017). The system-level impacts of such failures include substantial costs from replacements and downtime, as well as material end-of-life challenges that undermine the economic and environmental sustainability of wind farms. These issues underscore the urgent need for advanced monitoring, data-driven process optimization, and robust manufacturing control to ensure the structural integrity and longevity of wind turbine blades (Mikindani et al., 2025).

In composite manufacturing, multizone heating systems are increasingly used to enhance resin curing quality, particularly in large and inhomogeneous structures such as wind turbine blades. By dividing the mold into several independently controlled heating zones, these systems minimize the temperature gradients and promote uniform resin viscosity, flow, and curing across varying laminate thicknesses. This approach effectively reduces common defects, such as incomplete wet-out, dry spots, and residual stresses, caused by uneven thermal profiles. Previous investigations have shown that multizone improves both process reliability and mechanical performance by providing precise control of exothermic reactions during curingand allowing tailored hearing strategies for different blade sections(root, mid-span, and tip), which often differ in geometry and thickness (Liu et al., 2021; Yao et al., 2023).

Although high-fidelity simulations have proven effective for predicting the degree of cure and other thermomechanical phenomena (Ma et al., 2017; Shojaei et al., 2003), exploring the vast combinations of zone temperatures and heating history for optimization of the VARIM process remains a computationally demanding challenge in practical applications. To address

https://doi.org/10.5194/wes-2025-226
Preprint. Discussion started: 12 November 2025
© Author(s) 2025. CC BY 4.0 License.

this critical challenge, we propose a machine learning enabled digital twin approach to optimizing the VARIM process. This data-driven approach leverages the significant development in deep learning neural networks (DNNs) and, particularly, Long Short-Term Memory (LSTM) architectures. LSTM have attracted considerable attention for their ability to capture complex underlying principles across various domains such as machine health [7], virus mobility and infection prediction (Muñoz-Organero, 2022), brain tumor classification (Montaha et al., 2022), deformations in composites during curing (Feng et al., 2024), and proposed as digital twins (Tao et al., 2018; Zhang et al., 2024) in smart manufacturing (Kusiak, 2018), active manufacturing control for composites (Humfeld et al., 2021), as well as in temperature, residual stress, and distortion modeling for composites (Xu et al., 2024). Compared to conventional neural networks, LSTMs possess the capability to learn the time-series dynamics, thereby capturing the underlying temporal features of complex manufacturing processes.

This study extends the preliminary work presented in (Kamath et al., 2024), where a computational proof of concept of the digital twin–based curing framework was introduced. In this proposed framework, the digital twin of the VARIM process is established by integrating physics-based models with LSTM networks. This integration is critical: while physics-based models offer high accuracy, they are computationally expensive for simulating the coupled multiphysics interactions in composite curing. In contrast, a well-trained LSTM provides a universal approximation capability, efficiently capturing the nonlinear mapping between processing parameters and material responses. When coupled with an optimization algorithm, the digital twin can identify optimal temperature setpoints for multizone heating configurations, ensuring uniform curing, enhanced process efficiency, and improved product quality. The rest of the paper is organized as follows: Section 2 outlines the modeling approach, which includes both the Multiphysics model and the data-driven LSTM model for the digital twin. We then present a gradient-free optimization method for obtaining the optimal curing cycle. The developed modeling approach is validated through an experiment featuring a 3-zone VARIM setup as described in Section 3. The effectiveness of the ML-based digital twin is demonstrated in Section 4, followed by conclusions in Section 5.

2 Methodology

2.1 Governing equations of the VARIM process

In the VARIM process, the resin infuses into the fiber matrix and cures under the heat. This process is governed by a complex coupling of physical phenomena, including curing kinetics, thermo-fluid dynamics, and thermo-mechanical responses. To accurately simulate these coupled processes, this study utilizes the commercial software PAM-RTM. The primary focus is on the interaction between thermo-fluidic behavior and curing kinetics, which are critical to predicting the evolution of the degree of cure and thermal gradients during the VARIM process. In infusion-based curing processes, the flow of polymeric resin through the fiber preform is described by Darcy's law:

$$[\mathbf{v}] = -\frac{1}{\mu}[\mathbf{K}][\nabla p] \tag{1}$$

https://doi.org/10.5194/wes-2025-226
Preprint. Discussion started: 12 November 2025
© Author(s) 2025. CC BY 4.0 License.

in which [**v**] is the velocity vector, μ is viscosity assuming Newtonian flow, the matrix [**K**] is known as the permeability tensor, p is pressure and ∇ is the gradient operator.

The thermal/chemical equation is given by

$$\rho C_p \frac{\partial T}{\partial t} + \rho_r C_{pr} \mathbf{v} \cdot \nabla T = \nabla \cdot (\boldsymbol{\kappa} \cdot \nabla T) - \rho_r \Delta h \frac{da}{dt} \tag{2}$$

in which ρ and ρ_r are the mass densities of the composite and epoxy resin, respectively; C_p and C_{pr} are the specific heat of the composite and epoxy resin, respectively; T is temperature, $\mathbf{v}$ is the flow velocity. The second term represents the convection effects, the third term is the diffusion term with $\boldsymbol{\kappa}$ the conductance matrix, and the last term is due to the chemical reaction in which Δh is the enthalpy of resin polymerization and α is the curing degree resolved from the kinetic model. Heat convection is described by Newton's law of cooling,

$$\dot{Q} = hA\Delta T(t) \tag{3}$$

where $\dot{Q}$ is the heat transfer rate, h is the convective heat transfer coefficient, A is heat transfer surface area, and $\Delta T(t)$ The temperature difference between the environment and the composite laminate made in the VARIM is a time-dependent value.

The curing degree is governed by the kinetic equation, given as

$$\dot{\alpha} = k(T) f(\alpha) \tag{4}$$

in which $\dot{\alpha}$ is the curing rate, $k(T)$ is a rate constant, and $f(\alpha)$ is a function of the degree of cure, as determined by experimental characterization results. (Šimon, 2004; Um et al., 2002)

A list of the model parameters in equations (1-3) are summarized in Table 1 along with their sources.

Material	**Model parameters**	**Source of data**
Epoxy resin	Coefficient of thermal conductivity [W/ (m · K)]	Differential scanning calorimetry (DSC) measurements
	Density (kg/m^3)	DSC measurements
	Newtonian viscosity (N · s/m^2)	DSC measurements
	Specific heat [kJ/ (kg · K)]	DSC measurements
	Enthalpy (kJ/kg)	DSC measurements
Glass fiber sheet	Permeability (m^2)	Infusion experiment
Resin-infused preform	Coefficient of thermal conductivity [W/(m · K)]/ Specific heat [kJ/(kg · K)]	Temperature data from thermocouples embedded in the system and RFID sensor tags embedded in the composite
Foam	Coefficient of thermal conductivity [W/(m · K)] /Specific heat [kJ/(kg · K)]	Temperature data from thermocouples embedded in the system and RFID

https://doi.org/10.5194/wes-2025-226
Preprint. Discussion started: 12 November 2025
© Author(s) 2025. CC BY 4.0 License.

		sensor tags embedded in the composite

Table 1: A summary of values used in the multiphysics solver and their sources

As shown in Table 1, parameters such as resin density, viscosity, and thermal properties can often be obtained from technical datasets or manufacturer specifications. However, other parameters, such as kinetic cure parameters and model coefficients, were experimentally validated and characterized. In the following, we describe the calibration of the kinetic model. The rate constant $k(T)$ in Eq. (4) can be further expressed by an Arrhenius equation,

$$k(T) = Ae^{-\frac{E_a}{RT}} \tag{5}$$

where A is the pre-exponential factor, E_a is the activation energy, R is the universal gas constant (8.314 $J/mol.°K$), and T is the absolute temperature [$°K$]. In this form, $f(\alpha)$ is "model-based," meaning that the reaction order (usually in the form of $(1-\alpha)^n$) should be established and known. Instead of using a model-based approach, we use a "model-free" approximation. Model-free means that $f(\alpha)$ will be determined and assumed inherently through experimental data, allowing for easier approximation methods.

The Friedman isoconversion curing kinetics model is given as,

$$\beta \frac{d\alpha}{dT} = A(\alpha)\, exp\left(-\frac{E_a(\alpha)}{RT}\right) f(\alpha) \tag{6}$$

in which β represents the heating rate. Once the parameters are identified by calibrating the modeling results against the experimental data, the degree of curing is calculated based on the given temperature history.

In this study, we use what is known as the Friedman isoconversional method for kinetic model calibration (Hardis, 2012; Tarani and Chrissafis, 2024; Venkatesh et al., 2013; Vyazovkin et al., 2011). The above model can be rewritten as

$$ln\left(\frac{d\alpha}{dt}\right) = ln[A(\alpha)\cdot f(\alpha)] - \frac{E(\alpha)}{R}\cdot\frac{1}{T} \tag{7}$$

This form of the equation facilitates easy calculation of the activation energy and pre-exponential factors through linear regression of ln(dα/dt) vs. 1/T. Here we store the set of values of activation energy $E(\alpha)$ and the coefficients of the pre-exponential term for each value of α. Differential Scanning Calorimetry (DSC) was employed at multiple heating rates to capture the heat flow associated with the resin's exothermic polymerization reaction as a function of temperature. Baseline correction was applied to the DSC curves to eliminate non-reactive heat contributions. The degree of cure, denoted as α, was computed by taking the ratio of the partial area under the heat flow curve at any time step to the total area corresponding to complete reaction.

To calibrate the kinetic model, the derivative $\frac{d\alpha}{dt}$ was evaluated, and a plot of $\ln\left(\frac{d\alpha}{dt}\right)$ versus $\frac{1}{T}$ was constructed for each conversion level α. From the slope and intercept of these linear regressions, the activation energy $E(\alpha)$ and the pre-exponential coefficient C were determined. These parameters were stored in structured lookup tables (in .csv format) for

https://doi.org/10.5194/wes-2025-226
Preprint. Discussion started: 12 November 2025
© Author(s) 2025. CC BY 4.0 License.

subsequent use in multiphysics simulations and training machine learning models. A comparison of the calibrated model against the DSC results is shown in Fig 1.

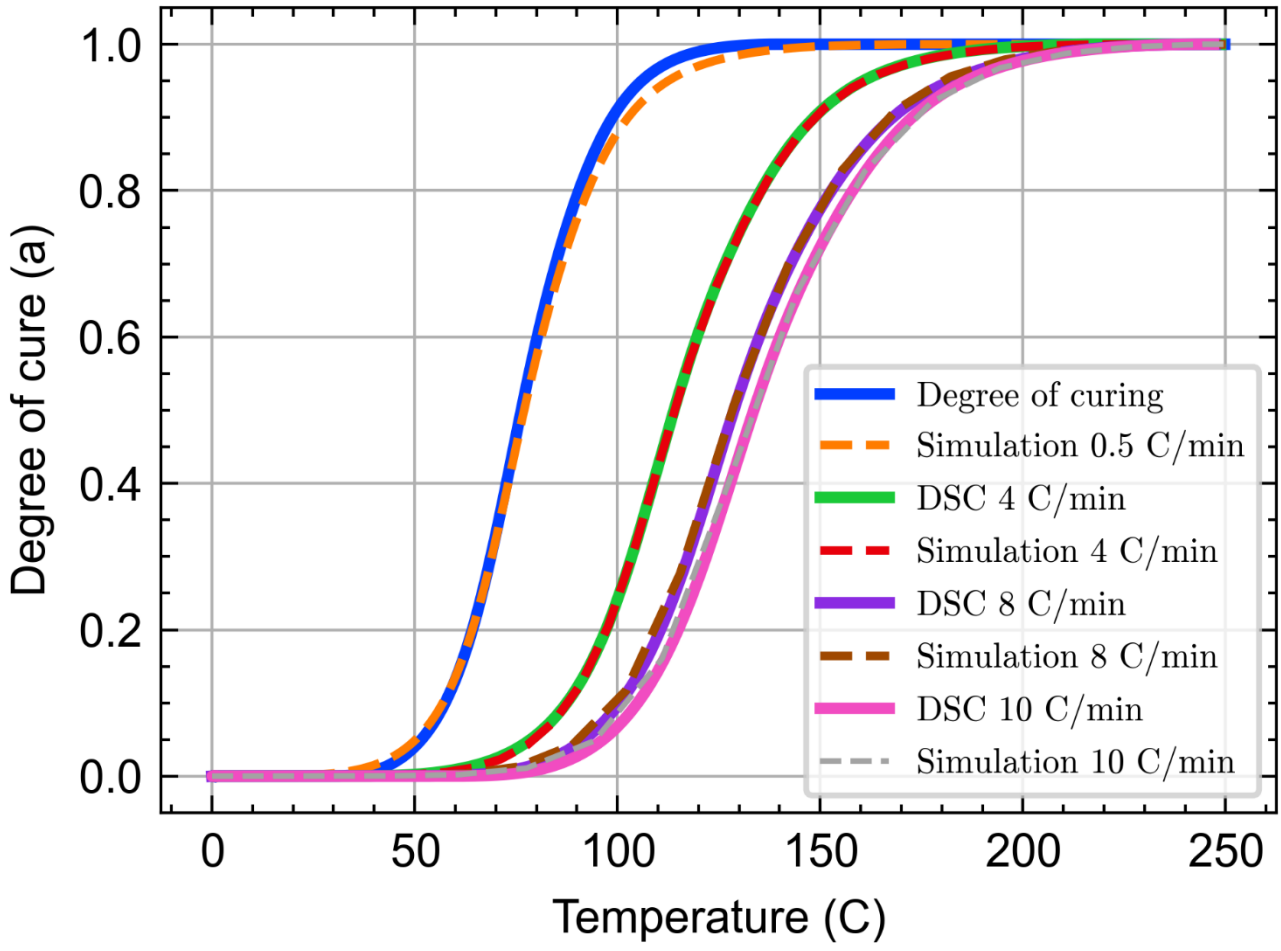

Figure 1: Comparing the calibrated model against Differential Scanning Calorimeter (DSC) plots.

2.2 A Machine Learning model for the VARIM process

The calibrated multiphysics model described in the previous section was used as a tool to generate large-scale datasets, establishing the machine learning model for the VARIM process as a digital twin. The choice of ML model greatly influences the accuracy and capabilities of the model. For this project, we have employed convolutional neural networks (CNN), recurrent neural networks (RNN), autoencoder decoder models, and/or combinations of these. CNN-RNN models are chosen due to their robustness in capturing complex spatio-temporal distributions. Among the various RNN models, this project makes use of long-short-term-memory (LSTM) ML models. LSTM layers of ML models adeptly capture the

https://doi.org/10.5194/wes-2025-226
Preprint. Discussion started: 12 November 2025
© Author(s) 2025. CC BY 4.0 License.

temporal dependencies within the sequential temperature data. The LSTM's unique memory cell mechanism allows it to retain and utilize information over extended periods, making it particularly effective for modeling the dynamic evolution of the curing process. The temperature from the curing process yields a time history curve, making LSTM a perfect option for handling this data.

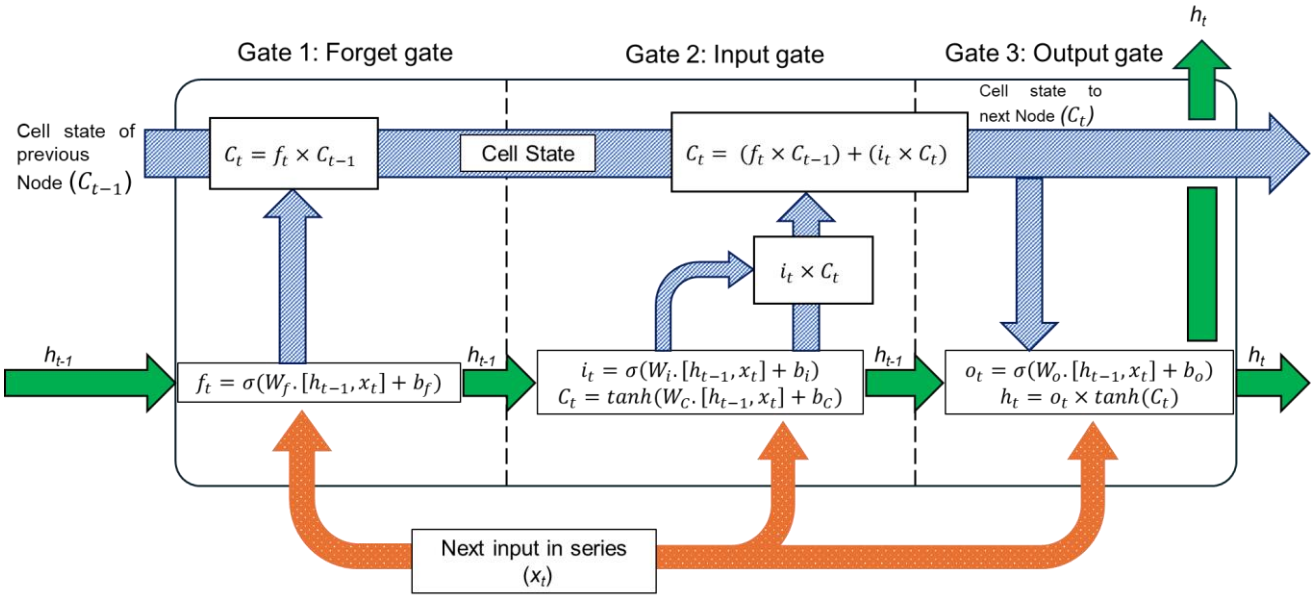

Figure 2: An illustration of the LSTM architecture.

The basic LSTM architecture is shown in Fig 2. LSTM networks retain long-term dependencies through three gates: the forget gate (f_t), input gate (i_t), and output gate (o_t), as defined in Equations (13)–(15) (F. Gers et al., 2002; F. A. Gers et al., 2000; Hochreiter and Schmidhuber, 1997). The cell state (C_{t-1}) provides a nearly linear path for information flow, allowing efficient preservation of past knowledge. The forget gate discards irrelevant information, and the input gate incorporates new information via the candidate vector $\tilde{C}_t$, and the output gate regulates the final output by filtering and scaling the updated cell state through a sigmoid and tanh activation functions. Detailed formulations of each step are given in Equations (8)– (12).

$$Gate\ 1: f_t = sigmoid\left(W_f \cdot [h_{t-1}, x_t] + b_f\right) \tag{8}$$

$$Gate\ 2: i_t = sigmoid(W_i \cdot [h_{t-1}, x_t] + b_i) \tag{9}$$

$$Gate\ 3: C_t = tanh(W_c \cdot [h_{t-1}, x_t] + b_c) \tag{10}$$

$$Gate\ 3: o_t = sigmoid(W_o \cdot [h_{t-1}, x_t] + b_o) \tag{11}$$

$$Gate\ 3: h_t = o_t \times tanh(C_t) \tag{12}$$

https://doi.org/10.5194/wes-2025-226
Preprint. Discussion started: 12 November 2025
© Author(s) 2025. CC BY 4.0 License.

The LSTM node is used in conjecture with fully connected dense layers, repeat vectors, and time-distributed dense layers, as shown in Fig 3. The model takes the temperature setpoint as the input and outputs the curing profile.

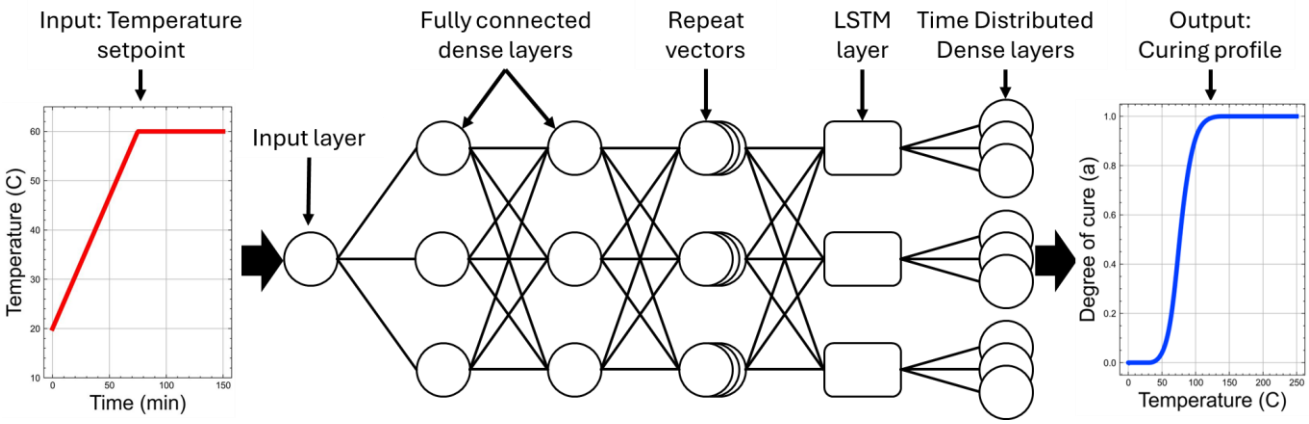

Figure 3: The ML model for the VARIM process.

The dataset used for training the forward machine learning (ML) model consists of physics-based simulated time-series data representing temperature and degree of cure in a multizone composite curing process. Each dataset (CSV file) includes temperature histories and corresponding curing responses for multiple heating zones. For the validation case, we have employed three heating zones—A, B, and C. Each zone of the heated bed is assigned a temperature setpoint, which is treated as a variable parameter. The temperature setpoints range from 50 °C to 80 °C, with a 1 °C interval in between, for each of the three zones, resulting in a dataset of 29,791 simulations. The temperature ranges were chosen based on the observation that temperatures exceeding 80 °C promote tool wear, whereas lower temperatures fail to initiate resin curing reliably.

The data are parsed, padded to a uniform sequence length, and stacked into 3D arrays suitable for sequence learning. Before training, input temperatures are normalized to ensure consistent numerical ranges across all zones, improving model stability and convergence. The output data, representing the degree of cure, are scaled using the same approach. The full dataset is then divided into training and testing subsets for model validation and performance evaluation.

The forward ML model is constructed as a sequential neural network, designed to capture both static relationships between temperature and cure, as well as temporal evolution throughout the heating process. It begins with a dense layer of neural network (10 units with L1 regularization and a LeakyReLU activation), which processes the scaled temperature inputs. This is followed by a layer that expands the input features along the time dimension to align with the output sequence length. At the core of the model is a Long Short-Term Memory (LSTM) layer (100 units with L1 regularization). The LSTM is critical because it retains information across time steps, learning temporal dependencies in the cure kinetics that simple feedforward networks cannot capture. It allows the network to recognize how past temperature variations influence current curing states.

https://doi.org/10.5194/wes-2025-226
Preprint. Discussion started: 12 November 2025
© Author(s) 2025. CC BY 4.0 License.

The output from the LSTM is passed through a dense layer with 50 units (L1 regularization), followed by a dense layer of a neural network (100 units with LeakyReLU activation). The TimeDistributed wrapper applies the same dense transformation at each time step, preserving the sequential structure and enabling the network to generate a full curing curve rather than a single-point prediction. The final TimeDistributed dense layer outputs degree-of-cure predictions for all three zones at every time step. The model is trained using the Adam optimizer and mean squared error (MSE) loss. Callbacks for learning rate reduction and early stopping are implemented to prevent overfitting and ensure convergence.

2.3 VARIM process optimization

Once trained, the forward machine learning (ML) model can predict the degree of cure for new temperature profiles, enabling its use as a surrogate in optimization workflows. The optimizer leverages these predictions to evaluate candidate temperature settings for each zone in the composite curing process. For every proposed temperature profile, the optimizer queries the ML model to generate time-series predictions of cure progression across all zones. These outputs are then used to compute an objective function that penalizes (1) the total time required to reach a target degree of cure (e.g., 90%) and (2) discrepancies in cure progression between zones—thereby promoting both efficiency and uniformity.

This objective function is minimized using the Nelder–Mead algorithm, a gradient-free optimization method well suited for non-differentiable or noisy problems. The algorithm begins with an initial simplex, which is an $(n+1)$-vertex structure in n-dimensional space (e.g., a tetrahedron for three temperature zones)—and iteratively refines it by reflecting, expanding, contracting, or shrinking the simplex based on the evaluated objective values. At each iteration, the ML model rapidly predicts the cure behavior for new candidate temperature profiles, allowing the optimizer to efficiently explore the design space without resorting to time-consuming physical experiments or high-fidelity simulations.

By integrating data-driven surrogate modeling with numerical optimization, this framework enables rapid identification of optimal cure cycles that minimize both process time and inter-zone non-uniformity. The approach offers a practical and computationally efficient tool for process engineers, facilitating the accelerated development and real-time optimization of composite manufacturing workflows.

3 Experimental Validation

3.1 Experimental setup

A laboratory-scale experimental setup was employed in this study to facilitate comprehensive data collection, model validation, and final product manufacturing as seen in Fig 4. This configuration featured three independently controlled heating zones, as specified by the project scope. This arrangement enabled the implementation and testing of optimized curing profiles generated by our framework under actual production conditions. The three-zone design provided sufficient spatial resolution to address the thermal variations encountered in the target composite structures while remaining practical from an implementation standpoint. Specifically, the setup consists of a 1.5m x 0.6m glass panel serving as the heating bed,

https://doi.org/10.5194/wes-2025-226
Preprint. Discussion started: 12 November 2025
© Author(s) 2025. CC BY 4.0 License.

mounted on a metallic frame with three separate chambers beneath to create three distinct heating zones. The chambers are heated by a 1500 W infrared bulb that maintains the given setpoint temperature in the zone. The heating elements are controlled by three relays, which are activated by an Arduino Uno microcontroller. Additionally, an RFID-based remote sensing setup is also used. This setup contains a set of antennae and remote sensing tags. The sensors provide a real-time output of the temperature, as well as a unique value called the sensor count difference error, which measures the change in dielectric constant of the material and indicates the progress in the resin polymerization reaction.

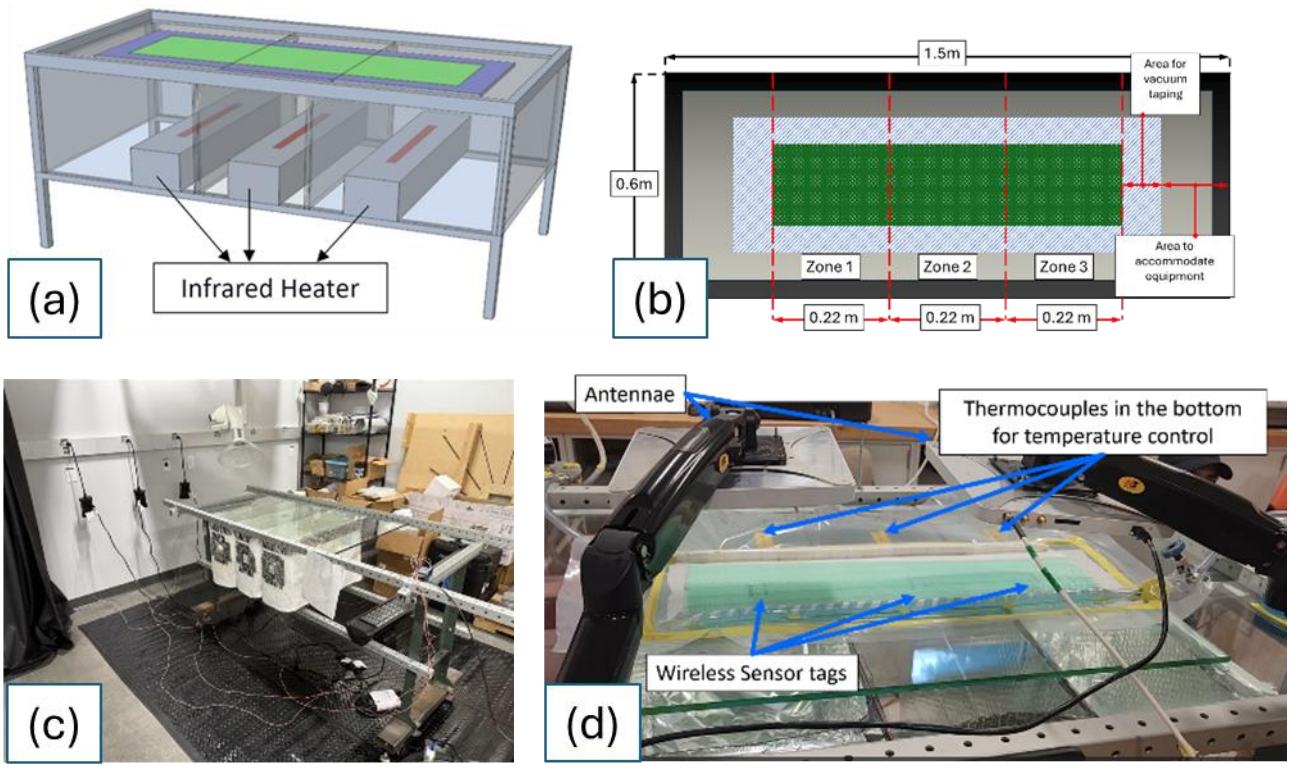

Figure 4: (a) A schematic of the experimental setup. (b) A top view of the infusion setup with three heating zones. (c) The experimental setup of the VARIM process and (d) Use of a wireless sensor for temperature sensing.

This setup was instrumented with six J-type thermocouples that could be positioned throughout the layup configuration, with data acquisition facilitated by a connected oscilloscope. The thermocouple array enabled precise monitoring of temperature gradients across the composite structure during the entire curing cycle, providing critical validation data for thermal model calibration. Three thermocouples were used to set the temperature boundary condition on the heated bed. At the same time, the other three were placed on top of the composite for data collection, validation, and safety. Temperature measurements were recorded at one-second intervals to capture transient thermal events during the polymerization process.

https://doi.org/10.5194/wes-2025-226
Preprint. Discussion started: 12 November 2025
© Author(s) 2025. CC BY 4.0 License.

3.2 Composite lay-up definition

A coupon design was chosen for manufacturing in a lab setting for validation, as shown in Fig 5 (above). Each composite plate was configured with three representative zones to mimic structural variations typical of large composite components. Zone A consisted of two layers of glass fibers. Zone B incorporated a tapered foam core sandwiched between two layers of glass fibers, creating localized thickness variations. Zone C used a uniform-thickness foam core between two glass layers, providing a baseline configuration. The resin system employed was Olin Airstone 780E combined with Olin Airstone 786H hardener.

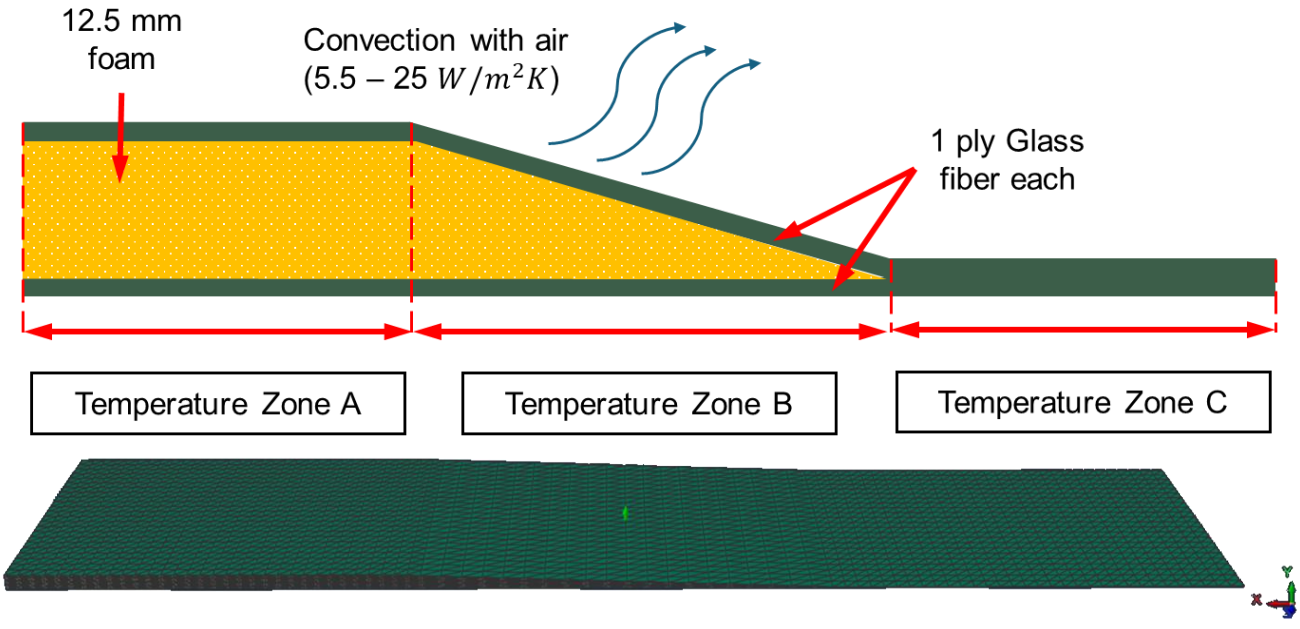

Figure 5: Coupon design to manufacture as a lab-scale proof of concept (top), Meshed model displayed in the PAM-Composites software (bottom).

3.3 Multiphysics Simulation

To generate the training dataset for the machine learning model, a high-fidelity finite element simulation of the VARIM process was conducted using the commercial software PAM-Composites. A CAD model representing the tapered composite laminate was developed and discretized using tetrahedral elements to ensure compatibility with Darcy's law, which governs the flow of resin through porous media. A fine mesh comprising 132,549 three-dimensional elements was selected to strike a balance between computational efficiency and simulation accuracy. Fig 5 (bottom) illustrates the meshed geometry within the PAM-Composites environment.

https://doi.org/10.5194/wes-2025-226
Preprint. Discussion started: 12 November 2025
© Author(s) 2025. CC BY 4.0 License.

Boundary conditions were applied to replicate realistic thermal environments encountered during the curing process. Specifically, nodes exposed to ambient air were assigned a convection boundary condition with a heat transfer coefficient ranging from 5.5 to 25 W/m²·K, reflecting the effects of natural convection. Meanwhile, nodes in contact with the heated bed were subjected to prescribed temperature curves corresponding to the setpoints of each independently controlled heating zone. These thermal boundary conditions were critical for accurately capturing the spatial and temporal evolution of temperature and degree of cure across the composite structure.

This simulation framework enabled the generation of a comprehensive dataset capturing the coupled thermo-fluidic and curing kinetics behavior under various multizone heating scenarios. The resulting data served as the foundation for training the machine learning-based digital twin described in subsequent sections.

4 Results and Discussion

4.1 Machine Learning and Optimization

The LSTM + Time Distributed ML model, used as a forward surrogate model, was trained on a workstation with an Intel Core i9-10900K CPU for a maximum of 100,000 epochs, with learning rate reduction on plateau and early stopping. The model converged at ~1100 epochs, depending on the initial seed. The trained model thus obtained performs at a mean error of 3.26% and a maximum error of 16.6% in outlier cases. An example of the predicted result is given in Fig 6. The total training time was 151mins for a model with 98,424 trainable parameters. Once fully trained, the forward surrogate model is capable of providing predictions (inference) within 0.4 seconds. Based on the trained forward surrogate model, process optimization was performed following the methodology described in section 2.3. The workflow presented iterates until the curing time is minimal and the difference between the curing rates of zones A, B, and C is as similar as possible. The results of the optimization were 67.77ºC, 62.67ºC, and 60.00ºC for the three respective zones. When these values were provided as inputs to the multiphysics solver, the curing rates were evaluated and plotted as shown in Fig 6, along with the predictions made by the ML model for the same values. Fig 7 illustrates the combined curing rates of the three zones. The results show good agreement between the ML model and the multiphysics solver, and the curing rates of the three zones overlap considerably at all time instances, proving that the curing rates over the part are uniform.

https://doi.org/10.5194/wes-2025-226
Preprint. Discussion started: 12 November 2025
© Author(s) 2025. CC BY 4.0 License.

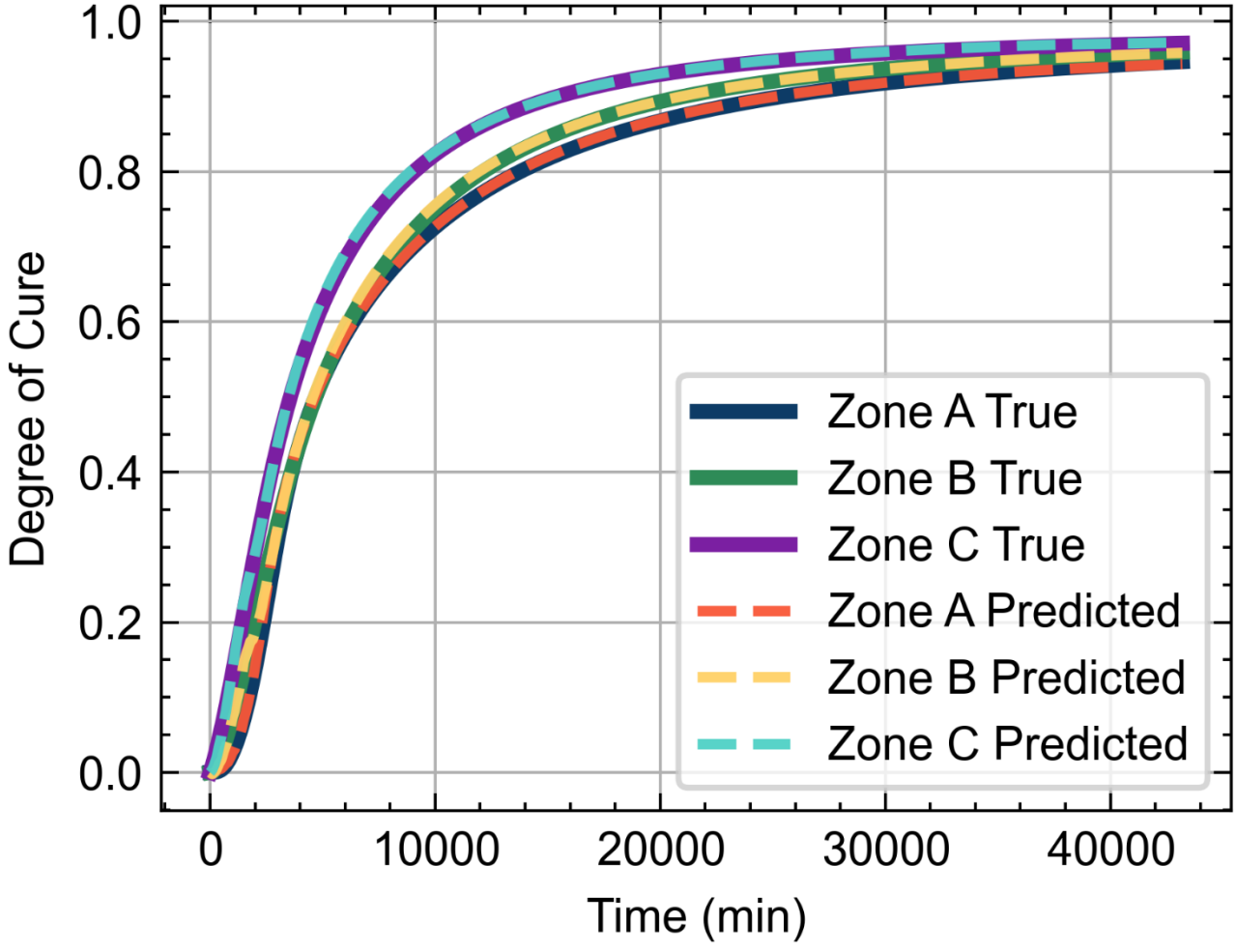

Figure 6: Predictions of the forward ML model compared to the ground truth from the multiphysics simulations.

https://doi.org/10.5194/wes-2025-226
Preprint. Discussion started: 12 November 2025
© Author(s) 2025. CC BY 4.0 License.

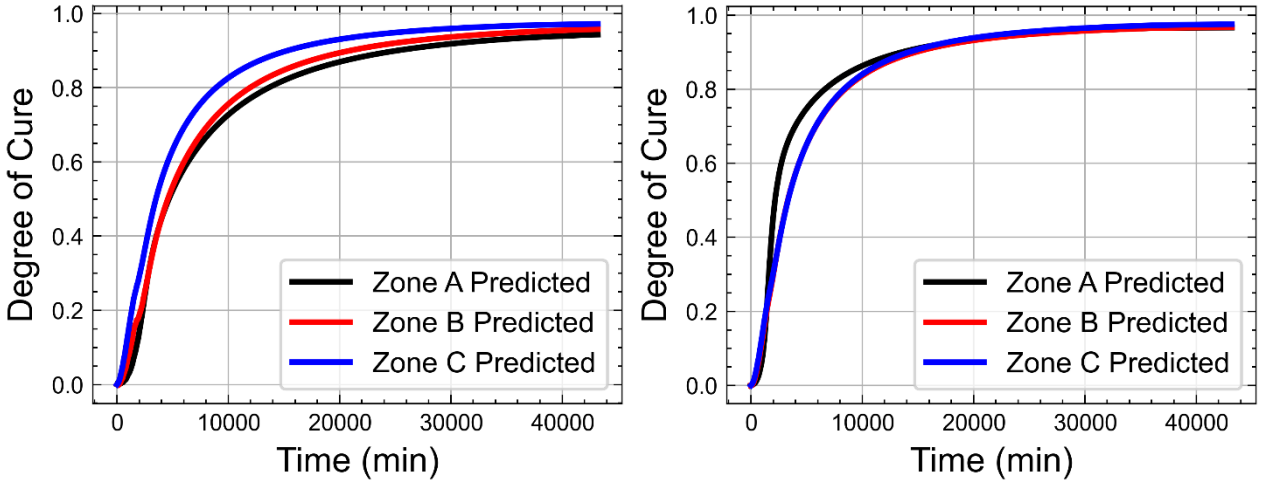

Figure 7: Degree of cure plots of the three zones for the conventional method (left) vs the optimized method (right).

4.2 Experimental validation

To evaluate the role of uniform curing on the improvements of mechanical performance of glass fiber epoxy composite sandwich structures, Combined Load Compression (CLC) tests were conducted under compressive loading, as illustrated in Fig 8. Two sets of specimens were prepared: one with a uniform degree of cure (UDOC) and the other with a non-uniform degree of cure (NUDOC). The purpose was to investigate how variations in the curing process impact the compressive modulus, yield strength, and ultimate strength, which are key mechanical indicators of stiffness and strength. Each specimen was subjected to compression testing to determine its compression modulus, yield strength, and ultimate strength. The yield strength was defined as the stress level at which the material begins to deform plastically, representing the transition from elastic to inelastic behavior.

https://doi.org/10.5194/wes-2025-226
Preprint. Discussion started: 12 November 2025
© Author(s) 2025. CC BY 4.0 License.

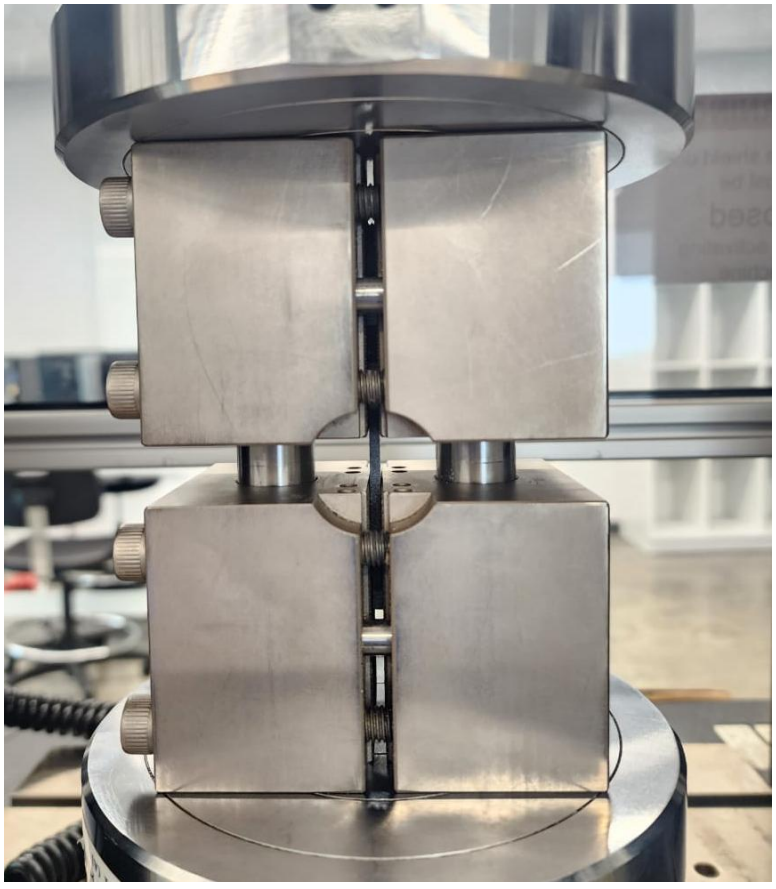

Figure 8: CLC test setup showing the composite attached.

To ensure accurate measurements of the compressive modulus, yield strength, and ultimate compressive strength, compliance correction was applied. Compliance represents the deformation per unit load, and the flexibility of the testing system must be accounted for to isolate the material's intrinsic stiffness. By correcting for compliance, the results more accurately reflected the inherent mechanical properties of the glass fiber/epoxy resin laminates, thereby eliminating the influence of the test apparatus's compliance.

Kink bands were observed in both UDOC and NUDOC specimens, as shown in Fig 9. These localized deformation zones form when aligned fibers collectively rotate and buckle under high compressive stress. This kinking failure mechanism is critical and frequently observed in structural composite applications such as wind turbine blades, where major load-bearing components (e.g., spar caps) experience severe cyclic compressive loading. The CLC test effectively replicates these complex combined stress conditions that can trigger such failure modes.

https://doi.org/10.5194/wes-2025-226
Preprint. Discussion started: 12 November 2025
© Author(s) 2025. CC BY 4.0 License.

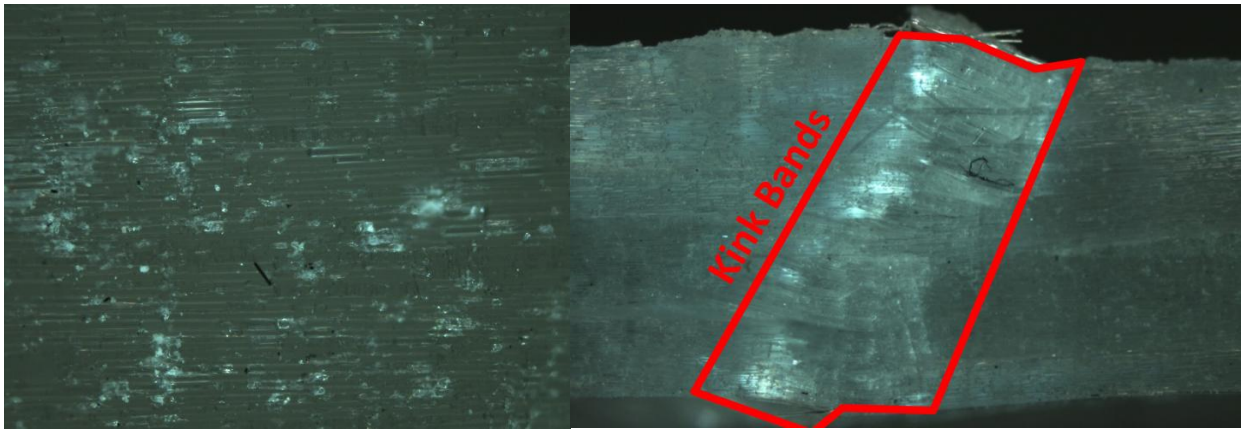

Figure 9: Micrograph showing aligned fibers before CLC test (left), and kink bands formed after CLC test (right).

The CLC test is susceptible to microscopic local imperfections, which are particularly prevalent in glass fiber-reinforced polymers (GFRPs). Failure modes, such as fiber micro-buckling, matrix cracking, and fiber-matrix debonding, occur more readily when defects, including uncured regions, fiber misalignment, voids, or dry spots, are present. These imperfections facilitate premature failure under compression, leading to a noticeable reduction in both strength and modulus. Although kink bands were observed in both specimen groups, their severity and effect were significantly greater in the NUDOC specimens due to the higher occurrence of such imperfections.

Specimen/Property	Yield Strength (MPa)	Ultimate Compressive Strength (MPa)
UDOC_1	51.89	460.85
UDOC_2	90.6	467.95
NUDOC_1	22.3	439.02
NUDOC_2	42.8	441.64

Table 2: Compressive yield strength and ultimate strength determined in CLC tests.

The CLC test results revealed a pronounced difference in mechanical performance between specimens with a uniform degree of cure (UDOC) and those with a non-uniform degree of cure (NUDOC), as summarized in Table 2. The UDOC specimens exhibited significantly higher stiffness, with an average compressive modulus 92.8% higher than the NUDOC specimens. Additionally, UDOC specimens showed an average ultimate compressive strength of 464.4 MPa compared to 440.3 MPa for the NUDOC specimens, representing a 5.5% increase.

Similarly, the yield strength of UDOC specimens averaged 71.25 MPa, substantially greater than the 32.55 MPa measured for NUDOC specimens, corresponding to an average percent difference of 74.6%. These pronounced reductions in both

https://doi.org/10.5194/wes-2025-226
Preprint. Discussion started: 12 November 2025
© Author(s) 2025. CC BY 4.0 License.

modulus and yield strength for the non-uniformly cured laminates are clearly illustrated in Fig 10, revealing the detrimental impact of curing non-uniformly on the mechanical performance of glass fiber/epoxy composites.

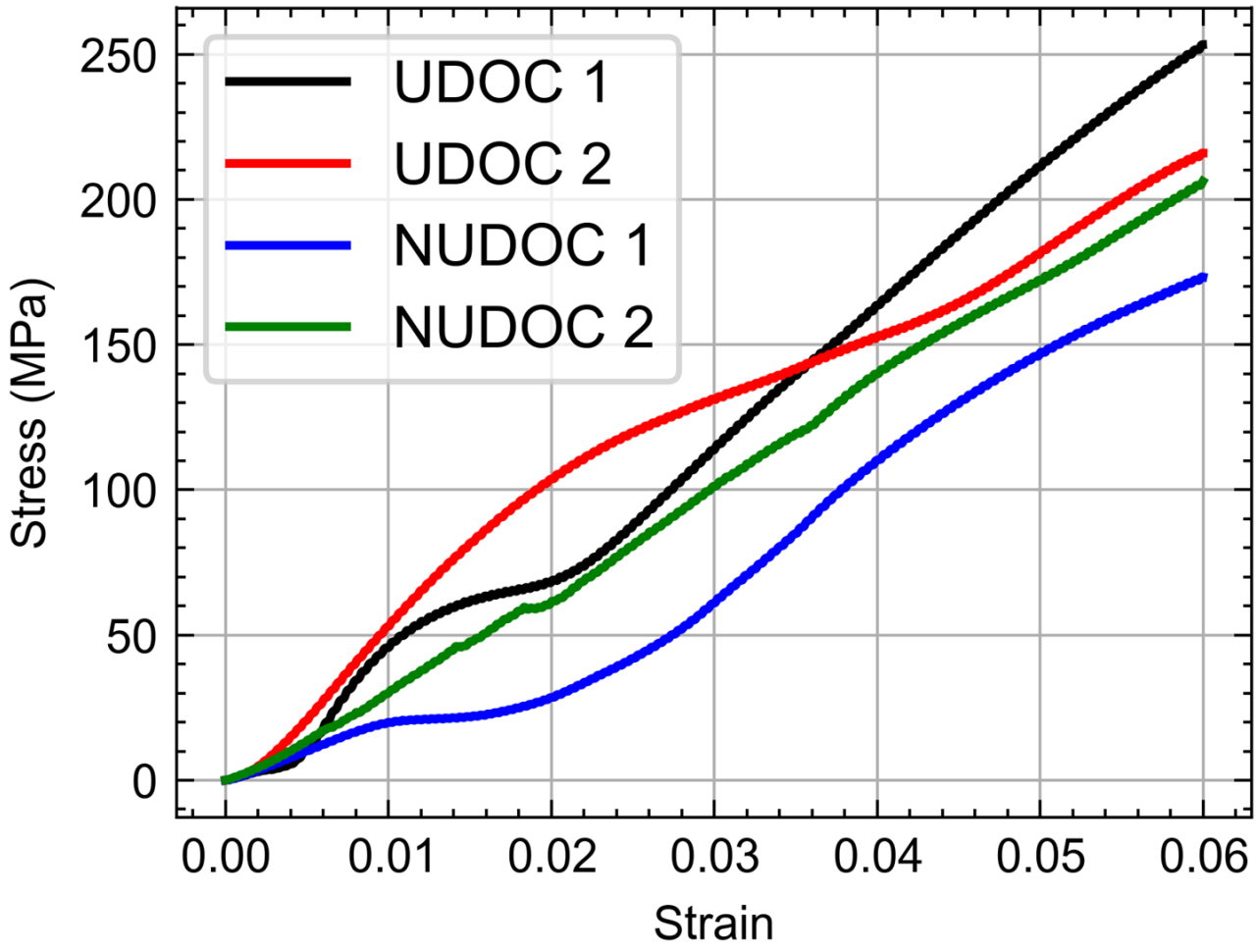

Figure 10: Stress – strain response of UDOC and NUDOC specimens under compression up to 6% compressive strain.

5 Conclusion

This work validates the effectiveness of LSTM-based models in capturing the complex temporal dynamics of resin curing and demonstrates the feasibility of employing machine learning models as surrogate models within optimization framework. The proposed approach successfully optimized curing cycle times for composites with varying thicknesses, representative of those used in wind turbine blades. While validation was conducted on a lab-scale sample, the algorithm can be scaled up to full-scale blade manufacturing. Once trained, the machine learning model can make instantaneous predictions, serving as a digital twin that replaces computationally expensive multiphysics simulations and iterative temperature setpoint evaluations.

https://doi.org/10.5194/wes-2025-226
Preprint. Discussion started: 12 November 2025
© Author(s) 2025. CC BY 4.0 License.

Consequently, the ML-based optimization framework is both scalable and reproducible. These findings mark a significant advancement forward improving efficiency, reliability, and performance in composite manufacturing processes.

Data availability

All raw data can be provided by the corresponding authors upon request.

Author Contributions

Sahil Kamath, Niloufar Adab, Rajat Srivastava, Zhiqi Mao, Ehsan Mehrdad, Dr. Yingjian Liu, and Dr. Dong Qian conceptualized the idea of the framework, developed and designed the methodology, and wrote the manuscript. Niloufar Adab, Rajat Srivastava, Zhiqi Mao, conducted the experiments. Sahil Kamath and Dr. Yingjian Liu designed the codes and the software. Stephen Nolet, Joseph Wilson, and Dr. Xu Chen provided resources and industry knowledge of the process. Stephen Nolet, Joseph Wilson, Dr. Xu Chen, Dr. Hongbing Lu, Dr. Dong Qian provided supervision and mentorship during the project and reviewed the writing of the manuscript.

Acknowledgements

This paper is based upon work partially supported by the National Science Foundation under 1362033 and 1916776 (I/UCRC for Wind Energy, Science, Technology, and Research) and from the members of WindSTAR I/UCRC. Any opinions, findings, conclusions, or recommendations expressed in this material are those of the authors and do not necessarily reflect the views of the National Science Foundation. The partial support of UTD Wind is gratefully acknowledged.

We would also like to acknowledge DOE under DE-EE0011016 for additional support. H. Lu also thanks the Louis A. Beecherl, Jr. Chair for additional support.

References

Feng, Y., Han, Z., Liu, M., Zheng, W., Liang, B., Xiong, Y., and Zhang, W.: Rapid prediction for deflection history of CFRP beams during curing using LSTM network and its application to stacking sequence optimization with genetic algorithm, Composites Part A: Applied Science and Manufacturing, 182, 108195, https://doi.org/10.1016/j.compositesa.2024.108195, 2024.

Fu, Y. and Yao, X.: A review on manufacturing defects and their detection of fiber reinforced resin matrix composites, Composites Part C: Open Access, 8, 100276, https://doi.org/10.1016/j.jcomc.2022.100276, 2022.

Hardis, R.: Cure kinetics characterization and monitoring of an epoxy resin for thick composite structures, Master of Science, Iowa State University, Digital Repository, Ames, https://doi.org/10.31274/etd-180810-1520, 2012.

© Author(s) 2025. CC BY 4.0 License.

Humfeld, K. D., Gu, D., Butler, G. A., Nelson, K., and Zobeiry, N.: A machine learning framework for real-time inverse modeling and multi-objective process optimization of composites for active manufacturing control, Composites Part B: Engineering, 223, 109150, https://doi.org/10.1016/j.compositesb.2021.109150, 2021.

Kamath, S., Caselato Gandia, G., Adab, N., Mehrdad, E., Qian, D., and Lu, H.: Machine-Learning Based Curing Cycle Optimization in Wind Blade Manufacturing, in: Volume 2: Advanced Manufacturing, ASME 2024 International Mechanical Engineering Congress and Exposition, Portland, Oregon, USA, V002T03A093, https://doi.org/10.1115/IMECE2024-146131, 2024.

Kedari, V. R., Farah, B. I., and Hsiao, K.-T.: Effects of vacuum pressure, inlet pressure, and mold temperature on the void content, volume fraction of polyester/e-glass fiber composites manufactured with VARTM process, Journal of Composite Materials, 45, 2727–2742, https://doi.org/10.1177/0021998311415442, 2011.

Kusiak, A.: Smart manufacturing, International Journal of Production Research, 56, 508–517, https://doi.org/10.1080/00207543.2017.1351644, 2018.

Liu, S., Li, Y., Shen, Y., and Goh, Y. M.: A Multi-Zoned Self-Resistance Electric Heating Method for Curing Irregular Fiber Reinforced Composite Parts, in: Advances in Transdisciplinary Engineering, edited by: Shafik, M. and Case, K., IOS Press, https://doi.org/10.3233/ATDE210028, 2021.

Ma, L., Athreya, S. R., Mehta, R., Barpanda, D., and Shafi, A.: Numerical modeling and experimental validation of nonisothermal resin infusion and cure processes in large composites, Journal of Reinforced Plastics and Composites, 36, 780–794, https://doi.org/10.1177/0731684417691673, 2017.

Maduro, M. A. M.: INFLUENCE OF CURING CYCLE ON THE BUILD-UP OF RESIDUAL STRESSES AND THE EFFECT ON THE MECHANICAL PERFORMANCE OF FIBRE COMPOSITES, 2021.

Mikindani, D., O'Brien, J., Leahy, P., and Deeney, P.: The financial risks from wind turbine failures: a value at risk approach, Applied Economics, 57, 6105–6120, https://doi.org/10.1080/00036846.2024.2380542, 2025.

Mishnaevsky, L.: Root Causes and Mechanisms of Failure of Wind Turbine Blades: Overview, Materials, 15, 2959, https://doi.org/10.3390/ma15092959, 2022.

Montaha, S., Azam, S., Rafid, A. K. M. R. H., Hasan, Md. Z., Karim, A., and Islam, A.: TimeDistributed-CNN-LSTM: A Hybrid Approach Combining CNN and LSTM to Classify Brain Tumor on 3D MRI Scans Performing Ablation Study, IEEE Access, 10, 60039–60059, https://doi.org/10.1109/ACCESS.2022.3179577, 2022.

Muñoz-Organero, M.: Space-Distributed Traffic-Enhanced LSTM-Based Machine Learning Model for COVID-19 Incidence Forecasting, Computational Intelligence and Neuroscience, 2022, 1–12, https://doi.org/10.1155/2022/4307708, 2022.

Shah, S. P., Olaya, M. N., Plaka, E., McDonald, J., Hansen, C. J., and Maiarù, M.: Effect of moisture absorption on curing of wind blades during repair, Composites Part A: Applied Science and Manufacturing, 173, 107706, https://doi.org/10.1016/j.compositesa.2023.107706, 2023.

Shojaei, A., Ghaffarian, S. R., and Karimian, S. M. H.: Modeling and simulation approaches in the resin transfer molding process: A review, Polymer Composites, 24, 525–544, https://doi.org/10.1002/pc.10050, 2003.

Šimon, P.: Isoconversional methods, Journal of Thermal Analysis and Calorimetry, 76, 123–132, https://doi.org/10.1023/B:JTAN.0000027811.80036.6c, 2004.

© Author(s) 2025. CC BY 4.0 License.

Struzziero, G., Nardi, D., Sinke, J., and Teuwen, J. J. E.: Cure-induced residual stresses for warpage reduction in thermoset laminates, Journal of Composite Materials, 54, 3055–3065, https://doi.org/10.1177/0021998320908631, 2020.

Tao, F., Qi, Q., Liu, A., and Kusiak, A.: Data-driven smart manufacturing, Journal of Manufacturing Systems, 48, 157–169, https://doi.org/10.1016/j.jmsy.2018.01.006, 2018.

Tarani, E. and Chrissafis, K.: Isoconversional methods: A powerful tool for kinetic analysis and the identification of experimental data quality, Thermochimica Acta, 733, 179690, https://doi.org/10.1016/j.tca.2024.179690, 2024.

Um, M.-K., Daniel, I. M., and Hwang, B.-S.: A study of cure kinetics by the use of dynamic differential scanning calorimetry, Composites Science and Technology, 62, 29–40, https://doi.org/10.1016/S0266-3538(01)00188-9, 2002.

Upadhyaya, P., Roy, S., Haque, M. H., and Lu, H.: A novel numerical–experimental approach for predicting delamination in high temperature polymer matrix composites, Composite Structures, 104, 118–124, https://doi.org/10.1016/j.compstruct.2013.04.008, 2013.

Venkatesh, M., Ravi, P., and Tewari, S. P.: Isoconversional Kinetic Analysis of Decomposition of Nitroimidazoles: Friedman method vs Flynn–Wall–Ozawa Method, J. Phys. Chem. A, 117, 10162–10169, https://doi.org/10.1021/jp407526r, 2013.

Vyazovkin, S., Burnham, A. K., Criado, J. M., Pérez-Maqueda, L. A., Popescu, C., and Sbirrazzuoli, N.: ICTAC Kinetics Committee recommendations for performing kinetic computations on thermal analysis data, Thermochimica Acta, 520, 1–19, https://doi.org/10.1016/j.tca.2011.03.034, 2011.

Wang, X., Wang, Q., Gao, L., and Jia, Y.: Effect of Heat Treatment on Curing Uniformity of Fiber Composite Laminates, Polymers and Polymer Composites, 25, 29–34, https://doi.org/10.1177/096739111702500105, 2017.

Wisnom, M. R., Gigliotti, M., Ersoy, N., Campbell, M., and Potter, K. D.: Mechanisms generating residual stresses and distortion during manufacture of polymer–matrix composite structures, Composites Part A: Applied Science and Manufacturing, 37, 522–529, https://doi.org/10.1016/j.compositesa.2005.05.019, 2006.

Xu, Y., Zhao, Z., Shrestha, K., Seneviratne, W., Liyanage, S., Palliyaguru, U., Karuppiah, A., Lua, J., Phan, N., and Yan, J.: A coupled data-physics computational framework for temperature, residual stress, and distortion modeling in autoclave process of composite materials, Composites Part A: Applied Science and Manufacturing, 183, 108218, https://doi.org/10.1016/j.compositesa.2024.108218, 2024.

Yao, X., Wang, Y., Thorn, T. D. S., Huo, S., Papageorgiou, D. G., Liu, Y., Bilotti, E., and Zhang, H.: Tailored Out-of-Oven Energy Efficient Manufacturing of High-Performance Composites with Two-Stage Self-Regulating Heating via a Double Positive Temperature Coefficient Effect, ACS Appl. Mater. Interfaces, 15, 56265–56274, https://doi.org/10.1021/acsami.3c12901, 2023.

Zhang, R., Liu, Y., Zheng, T., Eddin, S., Nolet, S., Liang, Y.-L., Rezazadeh, S., Wilson, J., Lu, H., and Qian, D.: A fast spatio-temporal temperature predictor for vacuum assisted resin infusion molding process based on deep machine learning modeling, J Intell Manuf, 35, 1737–1764, https://doi.org/10.1007/s10845-023-02113-4, 2024.

Zhou, B., Yu, F., Li, H., and Xin, W.: A Quantitative Study on the Void Defects Evolving into Damage in Wind Turbine Blade Based on Internal Energy Storage, Applied Sciences, 10, 491, https://doi.org/10.3390/app10020491, 2020.